Available online at www.sciencedirect.com
SCIENCE DIRECT®
Nuclear Instruments and Methods in Physics Research A 513 (2003) 585–595
NUCLEAR INSTRUMENTS & METHODS IN PHYSICS RESEARCH Section A
www.elsevier.com/locate/nima

The RPI multiplicity detector response to γ-ray cascades following neutron capture in ^{149}Sm and ^{150}Sm

Shangwu Wang[a], M. Lubert[b,*], Y. Danon[b], N.C. Francis[b], R.C. Block[b], F. Bečvář[c], M. Krtička[c]

[a] *Department of Applied Physics, School of Science, National University of Defense Technology, Changsha, Hunan, 410073, People's Republic of China*

[b] *Department of Mechanical, Aerospace and Nuclear Engineering, Rensselear Polytechnic Institute, 110 8th Street, NES Building, Troy, NY 12180-3590, USA*

[c] *Faculty of Mathematics and Physics, Charles University, V Holešovičkách 2, CZ-180 00 Prague 8, Czech Republic*

Received 14 March 2001; received in revised form 10 March 2003; accepted 25 May 2003

Abstract

The response of the RPI 16-segment NaI(Tl) multiplicity detector system to the γ-rays following neutron radiative capture reactions is discussed. An algorithm which combines the Monte-Carlo γ-cascade code DICEBOX, based on the extreme statistical model, with the general MCNP(4C) Monte-Carlo particle transport computer program is presented. Two processes, the emission of the γ-cascades accompanying the individual events of the neutron capture and the subsequent γ-ray transport through the RPI multiplicity detector were modeled. The efficiency of the RPI system for detecting neutron capture in ^{149,150}Sm nuclei and the expected distributions of instrumental multiplicity were derived using the combined DICEBOX/MCNP(4C) code. Comparison with measured data is presented.

Keywords: (n, γ) reactions; Multiplicity spectra; Detector efficiency; Statistical model; Monte Carlo gamma ray transport

1. Introduction

Computer simulation of neutron physics experiments, based on the use of complex detector systems, can help the experimentalist understand, in detail, how these systems work. This is an important prerequisite for improving the usefulness of the observed data in order to learn more about the underlying physics of the neutron capture process. In particular, these simulations are applicable in the analysis of raw data obtained from the measurement of neutron capture cross-sections in the resonance energy region. These data, together with spectra of γ-rays accompanying neutron capture, provide information about the mechanism of the (n, γ) reactions and the decay properties of the compound nuclear levels at excitations near the threshold for neutron emission.

The RPI 16-segment NaI(Tl) multiplicity detector [1] has been designed for time-of-flight neutron capture measurements using a pulsed neutron beam. A relatively high efficiency, η, for the detection of neutron capture has been achieved

*Corresponding author. Tel.: 518-276-4011.
E-mail address: luberm@rpi.edu (M. Lubert).

0168-9002/$ - see front matter
doi:10.1016/S0168-9002(03)01941-7

by taking advantage of the multiplicity spectroscopy technique. However, for several reasons, the γ-detection efficiency of the *individual NaI(Tl) elements* can be significantly less than 100%. The response of any similar γ-detector system depends on:

(i) the detailed behavior of the γ-ray cascades following neutron capture in a nucleus of interest. The detection efficiency depends on the (n,γ) reaction studied and the neutron resonance spin and parity state,
(ii) the transport of the cascade γ-rays through the γ-sensitive elements of the detector system (in this case, the NaI(Tl) crystals), as well as through the structural material.

It is important to know the value of η to avoid systematic errors in determining the capture cross-section from neutron time-of-flight measurements. It is clear, since η depends on both the properties of the detection system and the γ-cascade process, that the only way to solve this problem is to estimate η from simulations involving both processes. This requires modeling the emission of the γ-cascades and their subsequent interactions with the passive and active material of the detection system including the sample itself.

An algorithm was developed for this simulation, similar to that reported in Ref. [2], which combines the program DICEBOX [3], a Monte-Carlo γ-cascade simulator based on the statistical model, with the MCNP(4C) Monte-Carlo particle transport code [4]. This combination makes it possible to simulate the Markovian process of γ de-excitation of the highly excited neutron-capturing states and subsequently track the emitted cascade γ-rays through the RPI multiplicity detector system to determine the γ-ray energy deposited in the individual scintillation crystals. The detection efficiency η can be determined for any spin and parity of the (n,γ) capturing state given a statistically large enough sample of γ-cascades.

A similar task has been performed to determine the response of the Karlsruhe 4π γ-detection system, consisting of 42 large-volume BaF_2 scintillation spectrometers. A modified DICEBOX algorithm [3] in combination with the CERN transport code GEANT [5] were utilized to simulate the detector response. Relevant details for this work can be found in Ref. [6].

The DICEBOX/MCNP(4C) simulations provide information about the number of NaI(Tl) modules triggered by a γ-ray cascade. This is known as the *instrumental* γ-multiplicity m. The predicted distribution of m can be compared with that obtained from experimental measurements. The degree of agreement between these two distributions may, in turn, serve as a criterion for accessing the reliability of the DICEBOX/MCNP(4C) calculations. This is very important, as there exists no *direct* way to test the correctness of the outlined simulations. The accuracy of the DICEBOX predictions can be checked independently from comparisons of predicted cascade-related observables obtained from other experiments. The data that can be used for this purpose are, e.g. the total radiation widths of neutron resonances [7], spectra of γ-rays following neutron capture that belong to two-step or multi-step cascades [8] and populations of low-lying levels or the ratios of these populations as a function of capturing-state spin and parity in the product nucleus [9].

The DICEBOX algorithm is briefly explained in Section 2. Some of the models for photon strength functions and the level density incorporated in the present version of the DICEBOX/MCNP(4C) code are specified in detail in Section 3 with emphasis on the description of photon strengths for spherical and transitional nuclei. Section 4 lists the most relevant characteristics of the RPI detector system. The linking of the DICEBOX algorithm to the MCNP(4C) program, including the way in which the detection efficiency η and the distribution of instrumental γ multiplicity m are calculated is described in Section 5. A comparison of DICEBOX/MCNP(4C) simulations for the $^{149,150}Sm(n,\gamma)^{150,151}Sm$ reactions and those obtained from measurements with the RPI detector system [10] are presented in Section 6.

2. The method used to simulate the γ-cascades

The DICEBOX algorithm models the inherent statistical behavior of γ-cascade emissions and the

statistical characteristics of a large number of presumably unmeasured intermediate nuclear levels in medium and heavy nuclei. This eliminates the computational difficulties which existed in previous approaches to model the γ-cascades [11,12]. The statistical nature of the de-excitation process, the Porter and Thomas [13] fluctuation of partial radiation widths and the Wigner [14] distribution of the level spacings are fully taken into account. The nuclear level density and photon strength functions are the only two remaining entities needed for simulating the emission of cascade γ-rays in neutron radiative capture reactions apart from a known decay pattern of the low-energy levels in the product nucleus.

The DICEBOX algorithm is based on the validity of the extreme statistical model. The main features of this program are described as follows:

(i) Below a certain critical energy $E_{\rm crit}$, a full set of experimentally determined discrete levels of the nucleus are known, including level energies, spins, parities and all branching intensities of depopulating transitions.

(ii) A full and presumably unknown set of nuclear energy levels above $E_{\rm crit}$ is represented by a random discretization of an a priori known level density formula $\rho(E, J^{\pi})$.

(iii) When mixing of various multipolarities is allowed by the selection rules, the partial radiation width $\Gamma_{a\gamma b}$ for a γ transition between level 'a' with $E_a > E_{\rm crit}$ and ending at level 'b' is assumed to be a random quantity whose expectation value is uniquely determined by the photon strength and level density functions. Specifically,

$$\Gamma_{a\gamma b} = \sum_{X,L} y_{XL}^2 (E_a - E_b)^{2L+1} \frac{S_{\gamma}^{(XL)}(E_a - E_b)}{\rho(E_a, J_a^{\pi_a})} \quad (1)$$

where $S_{\gamma}^{(XL)}(E_{\gamma})$ is the known photon strength function for a given γ-radiation type X (electric or magnetic) and multipolarity L. The summation is assumed over all allowed values X, L. The quantity y_{XL} is a random variable of normal distribution with a zero mean and a unit variance. The terms of the sum on the right-hand side of Eq. (1) follow the Porter–Thomas distribution, which is also the case of the widths $\Gamma_{a\gamma b}$ when no multipolarity mixing takes place.

(iv) Pairs of partial radiation widths $\Gamma_{a\gamma b}$ and $\Gamma_{a\gamma b'}$ with $b \neq b'$ are statistically independent.

(v) Each γ-cascade starts from the same neutron-capturing state with known quantum characteristics and ends at the ground state. These characteristics are the spin and parity assignment together with the excitation energy $E_0 = B_{\rm n} + E_{\rm n}$, where $B_{\rm n}$ is the neutron-binding energy and $E_{\rm n}$ is the neutron energy.

(vi) The role of electron conversion is taken fully into account which makes it possible to mark the transitions of each simulated cascade by a flag distinguishing between electrons and γ-rays. Thus, an event of neutron capture is generally followed by a mixed cascade, represented by γ-ray and conversion-electron transitions.

The discretization of the level density formula $\rho(E, J^{\pi})$ and the way of generating partial radiation widths $\Gamma_{a\gamma b}$ are described in Ref. [3].

In view of the role of electron-converted transitions, the discussions below define the term "cascade" as a mixed cascade, while the term "γ-cascade" means a set of all γ-rays accompanying a neutron capture event. The γ-rays, forming a γ-cascade, do not necessarily exhaust all the initial energy E_0.

As shown in Ref. [3], with the above-listed features (i)–(vi), the DICEBOX algorithm can simulate, in principle, any cascade-related observable such as the γ multiplicity, γ-ray spectra, populations of low-lying levels and the total radiation width.

3. The level density and photon strength functions

3.1. Level density formula

The DICEBOX program has several explicit level density formulas. The simulations presented in this paper are based on the widely used Back-Shifted Fermi Gas (BSFG) level density

formula [15–18]:

$$\rho(E,J^{\pi}) = f_{\pi}f_{J}\frac{e^{2\sqrt{a(E-E_1)}}}{12\sqrt{2}\sigma a^{1/4}(E-E_1)^{5/4}} \quad (2)$$

where a is the conventional shell-model level density parameter and E_1 is a back shift. The factor $f_{\pi} = \frac{1}{2}$ represents the probability that a randomly chosen level has a parity π, while f_J is the probability that a randomly chosen level has a spin J, specifically

$$f_J = \frac{2J+1}{2\sigma^2}e^{-(J+\frac{1}{2})^2/2\sigma^2}$$

where σ is a spin cut-off parameter [15],

$$\sigma = 0.2980A^{1/3}a^{1/4}(E-E_1)^{1/4}$$

and A is the mass number of the compound nucleus. The parameters E_1 and a used are 0.781 MeV and 18.136 MeV^{-1}, respectively [16].

For a set of levels with a fixed spin and a fixed parity, the probability density for the level interval $D_J = E - E'$ between two neighbouring levels of energies E and E' in the set is given by the well-known Wigner law

$$\frac{dP}{dD_J} = \frac{\pi D_J}{2\langle D_J\rangle^2}e^{-\pi D_J^2/(2\langle D_J\rangle)^2}, \quad (3)$$

where $\langle D_J\rangle = 1/\rho(E,J^{\pi})$ is the expectation value of D_J. The Wigner law has been fully taken into account in the discretization of the level density formula.

3.2. Photon strength functions

DICEBOX contains many explicit expressions for photon strength functions $S_{\gamma}^{(XL)}(E_{\gamma})$. Those strength functions considered to be relevant for spherical and transitional nuclei were used. Three multipolarities $E1$, $M1$ and $E2$ together with a mixture $M1+E2$ are considered in modeling the cascade de-excitation. Higher mutipolarities were neglected in view of their negligible role in neutron capture reactions.

3.2.1. $E1$ radiation

There are many choices for the $E1$ photon strength functions based on the giant dipole resonance model [19–32]. The strength function proposed in Ref. [22] was used for the cases of the ^{150,151}Sm nuclei. It approximates the $E1$ photon strength function at low γ-ray energies as follows:

$$S_{\gamma}^{(E1)}(E_{\gamma},E_f) = \frac{F_K}{3\pi^2\hbar^2c^2}\sum_{j=1}^{2}\frac{\sigma_{0j}E_{0j}\Gamma_{0j}\Gamma_j}{(E_{\gamma}^2-E_{0j}^2)^2} \quad (4)$$

where

$$\Gamma_j = \Gamma_{0j}\frac{E_{\gamma}^2+4\pi T_f^2}{E_{0j}^2}, \quad T_f = \sqrt{(E_f-\Delta)/a},$$

$$\text{and} \quad F_K = \frac{(1+2f_1/3)^{1/2}}{(1+2f)^{1/2}}.$$

Quantities σ_{0j}, E_{0j}, Γ_{0j} $(j=1,2)$ are Lorentzian giant dipole electric resonance parameters. The quantity E_f is the final state energy of the γ transition, E_{γ} the γ-ray energy, a the shell model level density parameter, Δ the pair energy and T_f the nuclear temperature. Finally, f_1 and f are Migdal parameters of the interaction between quasiparticles [22]. This photon strength function depends on E_f which differs from the Brink hypothesis [20] in its stringent formulation.

The expression for $S_{\gamma}^{(E1)}(E_{\gamma},E_f)$ is valid for the general case of non-spherical nuclei. The sum on the right-hand side of Eq. (4) has two terms, $j=1,2$, representing the two modes of counteroscillation of neutron and proton fluids. This sum reduces to only one term for spherical nuclei. The values adopted for free parameters entering the expression for $S_{\gamma}^{(E1)}$ are as follows [31]:

$$\Delta = 0.781 \text{ MeV}, \quad F_K = 0.7.$$

The parameters for ^{149}Sm + n are

$$E_{01} = 14.61 \text{ MeV}, \quad \Gamma_{01} = 5.97 \text{ MeV},$$
$$\sigma_{01} = 312 \text{ mb}.$$

The parameters for ^{150}Sm + n are

$$E_{01} = 12.38 \text{ MeV}, \quad \Gamma_{01} = 2.97 \text{ MeV},$$
$$\sigma_{01} = 176 \text{ mb},$$
$$E_{02} = 15.74 \text{ MeV}, \quad \Gamma_{02} = 5.22 \text{ MeV},$$
$$\sigma_{02} = 234 \text{ mb}.$$

3.2.2. $M1$ radiation

Two types of magnetic dipole resonances are considered to be responsible for the $M1$ photon strength. The first, is the giant dipole magnetic

resonance [19,20,25,26,33] that belongs to oscillations related to the shell-model spin-flip transitions between the single-particle states with $j = l \pm 1/2$ [34,35]. The second, which occurs only in deformed and transitional nuclei, is the so-called scissors resonance [36]. Each of these resonances is assumed to be of Lorentzian shape and satisfy the Brink hypothesis [20]. With these assumptions the $M1$ photon strength function takes the following explicit form:

$$S_\gamma^{(M1)}(E_\gamma) = \frac{1}{3\pi^2\hbar^2c^2}\frac{1}{E_\gamma}\sum_{i=1}^{2}\frac{E_\gamma\sigma_{m0i}\Gamma_{m0i}^2}{(E_\gamma^2 - E_{m0i}^2)^2 + E_\gamma^2\Gamma_{m0i}^2} \quad (5)$$

where the two sets of parameters σ_{m0j}, E_{m0j} and Γ_{m0j} for $j = 1, 2$ are the maximum cross-section, the energy at this maximum and the damping width, respectively.

For both nuclei studied the spin-flip resonance parameters were taken from Refs. [26,34,35]. Specifically

$$E_{m01} = 7.72 \text{ MeV}, \quad \Gamma_{m01} = 3.5 \text{ MeV} \quad \text{and} \quad \sigma_{m01} = 2.0 \text{ mb}.$$

The scissors resonance parameters we used are

$$E_{m02} = 3.0 \text{ MeV}, \quad \Gamma_{m02} = 0.6 \text{ MeV} \quad \text{and} \quad \sigma_{m02} = 0.2 \text{ mb}.$$

3.2.3. *E2 radiation*

There are a few options for the $E2$ photon strength function [21,26,37–39]. Of these, the single-particle model was adopted

$$S_\gamma^{(E2)}(E_\gamma) = k_{E2} \quad (6)$$

where k_{E2} is set to 1.0×10^{-10} MeV^{-5}. The intensities of $E2$ transitions or their admixtures are two to three orders of magnitude weaker than intensities of the $E1$ transitions for typical energies of the cascade γ-rays.

4. The RPI multiplicity detector

A multiplicity detector is an arrangement of several independent γ-ray detectors surrounding a sample. The RPI multiplicity detector is shown, schematically, in Fig. 1. It was designed mainly to measure the radiative capture cross-section of heavy nuclides. The multiplicity detector consists of 16 optically isolated sections of NaI(Tl) forming a cylindrical annulus. The NaI(Tl) annulus is a 30.5 cm × 30.5 cm (12 in × 12 in.) right circular cylinder with an 8.9 cm (3.5 in.) diameter axial hole. The cylinder is split perpendicularly across its axis into two rings, and each ring is divided into eight equal pie-shaped segments. Each segment is viewed by an RCA 8575 photomultiplier. This detector has a total volume of 20 l of NaI(Tl) and has an efficiency of approximately 75% for a 2 MeV γ-ray. The inside of the detector is lined with a B_4C ceramic sleeve which is enriched 98.4% in ^{10}B. The sleeve has an inside diameter of 6.35 cm (2.5 in.) and an outside diameter of 8.38 cm (3.3 in.), thus providing a B_4C shield approximately 1 cm thick.

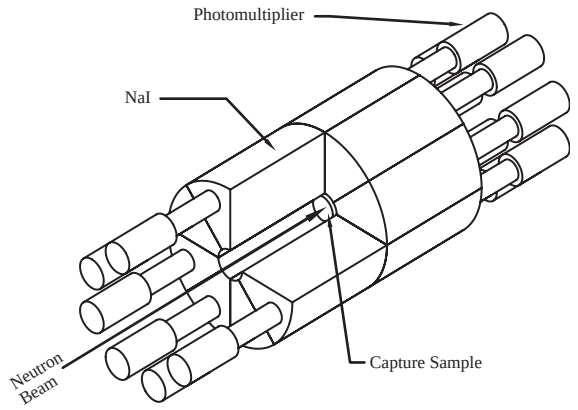

Fig. 1. RPI γ-multiplicity detector.

The detector measures, for each capture event, the γ energy deposited in each NaI(Tl) crystal. A specific capture event is logged if (1) sufficient energy is deposited in at least one NaI(Tl) segment that satisfies an experimental segment bias cut-off value and (2) the total energy deposited in *all* NaI(Tl) segments is higher than an experimental total energy bias cut-off value.

5. The simulation

When a γ-ray travels from its birth site to a detector segment, its energy could be degraded by

a number of interactions inside and outside the detector during the transport process. The mechanisms for energy loss outside the detector segments include: (1) collision energy loss in the target material, in the $^{10}B_4C$ liner and in the wrap materials of the NaI(Tl) crystals (aluminum and graphite); (2) loss due to escape of the γ-ray from the whole detector assembly. The escape of γ-rays and their collisions, occurring outside the NaI(Tl) segments, decrease the energy deposited in segments and, consequently, in the whole detector system, which results in a lower detection efficiency. The average *instrumental* γ multiplicity, m, is also affected.

A γ-cascade can trigger one or more detectors or none at all. In the general case, the number of γ transitions participating in a γ-cascade differs from the number of triggered detector modules. This implies that the distribution of *real* γ-cascade multiplicity differs from that of the *instrumental* multiplicity.

The simulation with the combined DICEBOX/MCNP(4C) algorithm consists of the following three steps:

Step 1. Creation of detector energy deposition tables: The MCNP(4C) code was used to track the emitted γ-rays through the RPI detector and the energy they deposit in each NaI(Tl) crystal. The model for tracking the γ-rays built into the MNCP(4C) algorithm assumes a monoenergetic isotropic γ-source, uniformly distributed in a sample, at the detector sample site. It tracks the random walk histories of these γ-rays through the detector geometry providing a step-by-step interaction account of each γ-ray from its birth to its death or escape.

An energy deposition table (EDT), based on MCNP(4C) γ-ray transport through the RPI detector system, was generated for a series of γ-ray energies E_{tab}. 19 EDT tables, each containing 9000 histories, were created for γ-rays energies $0.5\,\text{MeV} \leqslant E_{tab} \leqslant 9.5\,\text{MeV}$ with a step $\Delta E_{tab} = 0.5\,\text{MeV}$. These parameters are based on sensitivity studies in Ref. [2] which produced minimal granularity effects. Each EDT table contains the energy deposited in the 16 NaI(Tl) segments in a (9000×16) array. The sum of all 16 energy deposition entries in any EDT history can be anywhere between zero and E_{tab} (the initial energy of the source γ-ray), depending on how much energy has been lost due to the energy loss mechanisms.

Step 2. Energy deposition from a cascade: A γ-ray with energy E_γ is selected from a DICEBOX-generated cascade. An energy deposition table with the energy E_{tab} closest to E_γ is selected. A row is picked at random from this table. The energy deposited in each of the 16 detector segments by this γ-ray is obtained by multiplying the selected row by a scale factor E_γ/E_{tab}. The energy deposited in the detector segments for the other γ-rays in the cascade are obtained in the same way. The total energy deposited is obtained by summing the energy depositions in each detector segment from all γ-rays in a cascade. This process is repeated for each DICEBOX cascade. Hence for each cascade the energy deposited in each detector segment and the total energy absorbed are known.

Step 3. Getting the quantities of interest: The detection efficiency is determined from an inventory of those cascades that satisfy two threshold conditions: (1) the sum of all energies deposited in 16 segments by a cascade exceeds a total energy cut-off E_{tot}, (2) the energy deposited in at least one segment by a cascade exceeds the segment energy cut-off E_{seg}. The cases listed below result in zero instrumental multiplicity:

(i) The total energy deposited in 16 segments by a cascade is less than E_{tot}, but some segments receive an energy deposition greater than E_{seg}. This case is called a "zero cut-off by total energy".
(ii) The total energy deposited in 16 segments by a cascade is greater than E_{tot}, but no segment receives an energy deposition greater than E_{seg}. This case is called a "zero cut-off by segment".

In accordance with the standard adjustment of the RPI detector system, the experimental bias cut-offs were set to $E_{tot} = 1.0\,\text{MeV}$ and $E_{seg} = 0.1\,\text{MeV}$. All cascades which do not satisfy any of the listed instrumental zero multiplicity criteria are considered "detected". The simulated detection efficiency and the instrumental γ-multiplicity

spectrum are based on the statistics of these "detected" cascades.

The simulated detection efficiency η is determined from the following expression:

$$\eta = \frac{N_{cas} - N_{zero}}{N_{cas}} \times 100\%$$

where N_{cas} is the total number of cascades, N_{zero} is the number of cascades which contribute zero multiplicity.

The simulated *instrumental* γ-multiplicity distribution can be obtained in an analogous fashion. Denoting P_m to represent a probability of detecting a capture event with an instrumental multiplicity m, where $m \geqslant 1$, this quantity can be expressed as

$$P_m = \frac{N_m}{(N_{cas} - N_{zero})}.$$

Here, N_m represents the number of those cascades that satisfy the condition that the detector response is characterized by signals that exceed the segment energy cut-off E_{seg} in m detector modules, while the total signal exceeds the total cut-off E_{tot}.

6. Results of simulations

6.1. γ-multiplicity and detection efficiency

Table 1 lists the calculated results obtained from the simulated γ-cascades accompanying the ^{149,150}Sm(n, γ) ^{150,151}Sm reactions. The γ-cascades do not include internal conversion electrons. The probability of electron emission is not appreciable for energies $\geqslant$400 KeV so that penetration through the B_4C liner and wrap materials is negligible. They are included in the predicted Γ_γ and population of the low-lying levels. Values of predicted detector efficiency η of the RPI system are given as well as values of M and σ which characterize the γ-multiplicity distribution. M and σ are, respectively, the expectation value and the square root of the variance of this distribution. The predicted values of M and σ are given for those obtained from both the DICEBOX calculation alone and the DICEBOX/MCNP(4C) algorithm. The values of M, σ and η for the ^{149}Sm(n, γ) ^{150}Sm reaction are shown for the two possible spin and parity assignments J^π of the s-wave neutron-capturing states. The selection of the capturing state J^π is controlled in DICEBOX by the incident neutron energy selected.

Table 1 also includes values of M and σ obtained from ^{149,150}Sm(n, γ) ^{150,151}Sm measurements made with the RPI Linear Accelerator and detector system. The values of M for the two capturing spin states $J^\pi = 3^-, 4^-$ were obtained by sampling the $J^\pi = 3^-$ data at three resonances (12.01, 25.26 and 29.8 eV) and four $J^\pi = 4^-$ resonances (4.95, 8.95, 14.91 and 17.165 eV). The measured data for the ^{150}Sm(n, γ) reaction yielded a single resonance at 20.65 eV which could be used to extract a value of M for the $J^\pi = 1/2^+$ capturing state.

The simulated distributions of γ-multiplicity m for the ^{149}Sm(n, γ) ^{150}Sm reaction are displayed in

Table 1
The detector efficiency η of the RPI system and values of the parameters M and σ

Target	B_n (keV)	J^π	DICEBOX		DICEBOX/MCNP(4C)			Measured	
			M	σ	M	σ	η (%)	M	σ
^{149}Sm	7986	3^-	4.79[a]	1.07[a]	4.37	1.70	96.4±0.1	4.79±0.07	1.52
		4^-	5.20[b]	1.09[b]	4.66	1.70	96.7±0.1	4.99±0.05	1.62
^{150}Sm	5597	$1/2^+$	4.19[c]	1.10[c]	3.19	1.73	87.3±0.1	3.64±0.04	1.32

The expectation value and the square root of the variance of multiplicity distribution respectively, are given. These values are shown for the neutron-capturing states with specified J^π and neutron-binding energies B_n.

[a] From neutron capture at isolated $J^\pi = 3^-$ resonance with energy 6.43 eV.

[b] From thermal neutron capture dominated by 99.1% contribution from neutron resonances with $J^\pi = 4^-$.

[c] From thermal neutron capture; only neutron resonances with $J^\pi = 1/2^+$ are contributing.

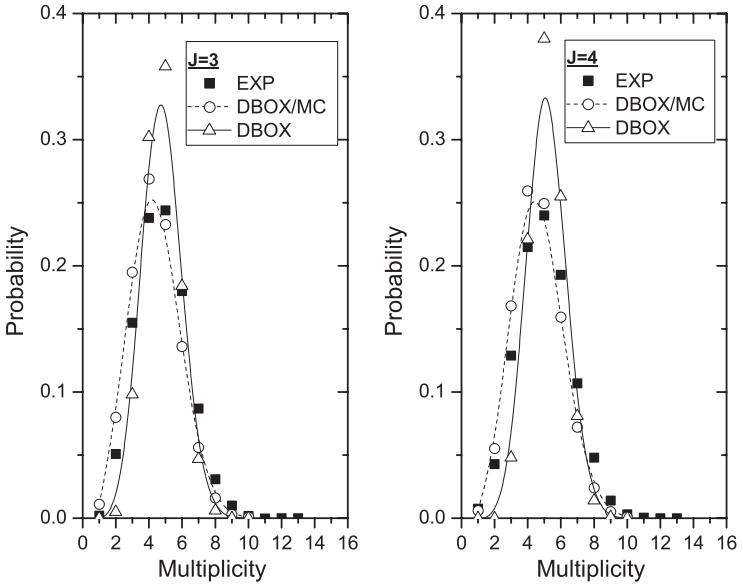

Fig. 2. The predicted multiplicity spectra for ^{150}Sm are compared with experimental data. The points are as calculated and the curves are spline fits to the simulated spectra. The experimental symbols include the error bars.

Fig. 2 and compared with the corresponding instrumental multiplicity distributions derived from the RPI measurements. The curve, *DBOX*, is the multiplicity predicted by DICEBOX. The second multiplicity curve, *DBOX/MC*, was obtained after transporting the cascade γ-rays through the detector.

6.2. Total radiation widths and populations of low-lying levels

The DICEBOX program also predicts the values of the total radiation widths Γ_γ for s-wave resonances in the ^{149}Sm(n, γ) and ^{150}Sm(n, γ) reactions. DICEBOX also provides data to predict the populations of the individual low-lying levels in ^{150}Sm resulting from the $J^\pi = 4^-$ thermal neutron-capturing state in the ^{149}Sm(n, γ) reaction. A detailed description for the basis of these predictions can be found in Ref. [3].

The predicted Γ_γ are presented in Table 2 for spin and parity assignments $J^\pi = 3^-$, 4^- and $J^\pi = 1/2^+$ of the neutron-capturing states for the ^{149}Sm(n, γ) and ^{150}Sm(n, γ) reactions, respectively. These are compared with the experimental values of Γ_γ, reported in Ref. [10]. The Γ_γ differences range from 18% to 26%.

Table 2
Total radiation width Γ_γ

Target	J^π	DICEBOX	MEASURED [10]
		Γ_γ (meV)	Γ_γ (meV)
^{149}Sm	3^-	76.6±0.69	62.3±4.0
^{149}Sm	4^-	73.5±0.68	58.2±1.4
^{150}Sm	$1/2^+$	37.07±0.11	45.0±4.0

The populations were estimated for 33 low-lying levels in ^{150}Sm of both parities with spin assignment covering the interval $J = [0, 8]$ and excitation energies below a critical value of $E_{crit} = 2.025$ MeV. The calculated value of population intensity for each level is compared with the sum of the intensities of all experimentally known transitions, depopulating that particular level. This comparison is shown in Fig. 3. The intensity values of the depopulating transitions were taken from Ref. [40]. These were renormalized using the data of Ref. [41] on *absolute* intensities of selected γ transitions following the thermal neutron capture

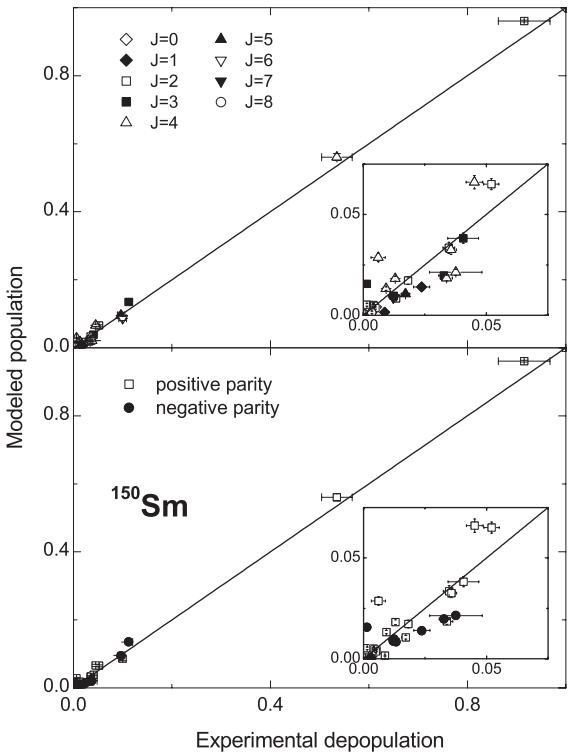

Fig. 3. Population of low-lying discrete levels for the nucleus ^{150}Sm.

in ^{149}Sm. It it important to note that plotted values of the simulated population and the measured depopulation in Fig. 3 are corrected for internal electron conversion contributions.

6.2.1. Discussion

Fig. 2 shows that predicted distributions of the instrumental γ multiplicity, belonging to the decay of $J^{\pi} = 3^{-}$ and $J^{\pi} = 4^{-}$ capturing states in the ^{150}Sm nucleus, differ only slightly from the corresponding measured distributions obtained with the RPI detection system. As can be seen from Table 1 the expectation values M of the instrumental γ multiplicity, obtained from simulations are lower than those measured. Although this difference, $M_{\mathrm{exp}} - M_{\mathrm{sim}} \simeq 0.5$ is small, it is statistically meaningful as are the above-mentioned differences between the simulated and the observed multiplicity distributions. On the other hand, as seen from Fig. 2 and from the values of the parameter σ in Table 1, the widths of the simulated distributions agree reasonably with measurements for the ^{149}Sm(n, γ) ^{150}Sm reaction.

It is worthwhile to note that the multiplicity distributions derived from "bare" DICEBOX simulations are narrower compared to those yielded by the combined DICEBOX/MCNP(4C) simulations. Further, their expectation values M are higher than those derived from the combined simulations. The influence of the γ-transport process on the observed γ multiplicity is thus prominent.

Looking at the results for the ^{149}Sm(n, γ) ^{150}Sm reaction in Table 1, simulated values of detection efficiency η do not display any marked dependence on the capturing state spin. The expectation values M and η depend on the specific capture reaction simulated.

It is worth noting that the $\sim$9.3% difference in detection efficiency between ^{149}Sm(n, γ) ^{150}Sm, $\sim$96.6%, and ^{150}Sm(n, γ) ^{151}Sm, $\sim$87.3%, is significant when determining the capture yield with the multiplicity detector. The capture data are usually normalized to unit yield, i.e. 100% of the neutrons are captured, in a low-energy saturated capture resonance. However, this normalization only applies to resonances for which the detection efficiency is the same. Thus, if the capture data are normalized to a saturated capture resonance in ^{149}Sm(n, γ) ^{150}Sm, then the capture yield in the ^{150}Sm(n, γ) ^{151}Sm resonances have to be renormalized to take into account the $\sim$9.3% differences in detection efficiencies. Simulation studies such as those presented in this paper will enable these isotope-to-isotope corrections to be made for capture experiments.

More than four decades have been devoted to the study of photon strength functions for medium-weight and heavy nuclei [24]. Nevertheless, current knowledge about the characteristics of the γ decay is still very limited because of experimental difficulties, especially in the γ-ray energy region below 3 MeV. The theoretical models for photon strength functions, described in Section 3, are thus to be regarded as "best" approximations. Similarly, the level-density formula, Eq. (2), is again our "best" estimate due to a lack of direct experimental information on the

density of nuclear levels with excitation energies from about 3 MeV up to the neutron threshold. The disagreement between the simulated and experimentally determined multiplicity distributions is, in fact, surprisingly small in view of the uncertainty in both crucial entities, responsible for emitting γ-cascades. A similar positive statement can also be made regarding the $\simeq 25\%$ difference between the predicted and observed total radiation widths Γ_γ in the $^{149,150}\mathrm{Sm}(\mathrm{n},\gamma)^{150,151}\mathrm{Sm}$ reactions, see Table 2.

7. Concluding remarks

The DICEBOX/MCNP(4C)-based algorithm for simulating the multiplicity detector response shares a unique position. Except for the case, reported in Ref. [6], it is evidently the only one which takes into account the role of all factors, responsible for production of *statistical* γ-cascades, accompanying individual events of neutron capture, as well as subsequent interactions of the emitted γ-rays with the complicated detection system. Notwithstanding the persisting limitations in knowledge of the photon strength functions, the estimates of detection efficiency η with the aid of the combined DICEBOX/MCNP(4C) algorithm seem to be precise enough for practical use in measurements of neutron capture cross-sections. Nevertheless the justifiability of the reported simulation method rises and falls with the validity of basic postulates of the extreme statistical model of the nucleus. Confidence in current or new nuclear models can be gained from DICEBOX/MCNP(4C) simulations as new γ multiplicity data using, multi-γ-detector systems, become available.

Acknowledgements

Two of the co-authors of this paper would like to express their thanks to the Rensselaer Polytechnic Institute Gaettner Laboratory—S.W. for providing an excellent research environment during the stay as a visiting scholar and F.B. for hospitality during a short visit.

This work was partly supported by the Grant Agency of the Czech Republic under contract no. 202/03/P136.

References

[1] R.C. Block, Y. Danon, R.E. Slovacek, C.J. Werner, G. Youk, in: International Conference on Nuclear Data for Science and Technology, Gatlinburg, TN, USA, 9–13 May, 1994, pp. 81–85.
[2] G. Leinweber, Ph.D. Thesis, Rensselaer Polytechnic Institute, Troy, 1994.
[3] F. Bečvář, Nucl. Instr. and Meth. A 417 (1998) 434.
[4] J.F. Briesmeister (Ed.), *MCNP*^{TM}—a general Monte-Carlo N-particle transport code, LA-12625-M, Version 4B, March 1997. RSICC Computer Code Documentation CCC-660, April 1997.
[5] J. Apostolakis, Technical Report, CERN, GEANT Library, 1993, www.cern.ch.
[6] R. Reifarth, M. Heil, F. Käppeler, F. Voss, K. Visshak, F. Bečvář, M. Krtička, R. Galino, Phys. Rev. C 66 (2002) 064603.
[7] J. Kopecky, Handbook for Calculations of Nuclear Reaction Data, IAEA-TECDOC-1034, August 1998, p. 97.
[8] F. Bečvář, in: S. Wender (Ed.), Capture Gamma-Ray Spectroscopy and Related Topics, AIP, New York, 2000, p. 504.
[9] L. Zanini, F. Corvi, H. Postma, F. Bečvář, M. Krtička, J. Honzátko, I. Tomandl, Phys. Rev. C 68 (2003) 014329.
[10] G. Leinweber, et al., Nucl. Sci. Eng. 142 (2002) 1.
[11] E.S. Troubetzkoy, Phys. Rev. 112 (1961) 212.
[12] D. Sperber, Phys. Rev. 142 (1966) 578.
[13] C.E. Porter, R.G. Thomas, Phys. Rev. 104 (1956) 483.
[14] E.P. Wigner, in: Proceedings of Conference on Neutron Physics by Time-of-Flight, Oak Ridge National Laboratory Report, Gatlinburg, TN, ORNL-2309, 1956.
[15] A. Gilbert, A.G.W. Cameron, Can. J. Phys. 43 (1965) 1446.
[16] T. von Egidy, H.H. Schmidt, A.N. Behkami, Nucl. Phys. A 481 (1988) 189.
[17] H.A. Bethe, Rev. Mod. Phys. 9 (1937) 69.
[18] W. Dilg, et al., Nucl. Phys. A 217 (1973) 269.
[19] P. Axel, Phys. Rev. 126 (1962) 671.
[20] D.M. Brink, in: F.E. Throw (Ed.), International Conference on Nuclear Physics with Reactor Neutrons, Argonne National Laboratory Argonne, IL, Report ANL-6797, 1963, p. 194.
[21] J. Kopecky, R.E. Chrien, Nucl. Phys. A 468 (1987) 285.
[22] S.G. Kadmensky, V.P. Markushev, V.I. Furman, Sov. J. Nucl. Phys. 37 (1983) 165.
[23] V.K. Sirotkin, Sov. J. Nucl. Phys. 43 (1986) 362.
[24] G.A. Bartholomew, Annu. Rev. Nucl. Sci. 11 (1961) 275.
[25] C.B. Dover, R.H. Lemmer, F.J. Hahne, Ann. Phys. 70 (1972) 458.

[26] J. Kopecky, M. Uhl, Phys. Rev. C 41 (1990) 1941.
[27] M. Uhl, et al., Int. Nucl. Data Comm. NDS 238 (1990) 113.
[28] M. Uhl, et al., Int. Nucl. Data Comm. NDS 335 (1995) 157.
[29] J. Kopecky, M. Uhl, R.E. Chrien, Phys. Rev. C 47 (1993) 312.
[30] B.L. Berman, At. Data Nucl. Data Tables 15 (1975) 319.
[31] S.S. Dietrich, B.L. Berman, At. Data Nucl. Data Tables 38 (1988) 199.
[32] M. Blatt, V.F. Weisskopf, Theoretical Nuclear Physics, Wiley, New York, 1952.
[33] D. Frekers, et al., Phys. Lett. B 244 (1990) 178.
[34] A.G. Bohr, B.R. Mottelson, Nuclear Structure, Vol. II, Benjamin, London, 1975, p. 636.
[35] S. Raman, et al., in: J. Speth (Ed.), Electric and Magnetic Giant Resonance in Nuclei, World Scientific, Singapore, 1991;
S. Raman, et al., Int. Rev. Nucl. Phys. 7 (1991) 356.
[36] A. Richter, Nucl. Phys. A 507 (1990) 99.
[37] N. LoIudice, F. Palumbo, Phys. Rev. Lett. 41 (1978) 1532.
[38] W.V. Prestwitch, M. Islam, T.J. Kennett, Z. Phys. A 315 (1984) 103.
[39] J. Speth, et al., Rep. Prog. Phys. 44 (1981) 719.
[40] E. derMateosian, J.K. Tuli, Nuclear Data Sheets 75 (1995) 827.
[41] M. Krtička, Ph.D. Thesis, Charles University, Prague, 2002.